Integrated crop growth and radiometric modeling to support Sentinel synthetic aperture radar observations of agricultural fields

Aaron Davitt[a,*] **Jonathan M. Winter**[b] **and Kyle McDonald**[c]
[a]City University of New York, The Graduate Center, Department of Earth and Environmental Sciences, New York, New York, United States
[b]Dartmouth College, Department of Geography, Hanover, New Hampshire, United States
[c]The City College of New York, New York, New York, United States

Abstract. Crop monitoring using synthetic aperture radar requires an understanding of how dynamic crop features influence radar response. We use crop parameters from the decision support system for agrotechnology transfer (DSSAT) model, a dynamic crop growth model, as inputs to the Michigan microwave canopy scattering (MIMICS) model, a radiometric model, to simulate radar scattering from selected wheat, rice, and corn fields in Yolo County, California, during 2015. We compared DSSAT-MIMICS modeled backscatter to Sentinel-1A backscatter and conducted sensitivity analyses to examine crop features that influence backscatter. For each crop, DSSAT-MIMICS modeled VV (vertically transmitted and received) backscatter was correlated to Sentinel-1A σ^0_{VV} (mean R-value $= 0.76$, $p < 0.05$), root-mean-square error <2 dB, and a model bias between −0.23 and 0.99 dB. However, there were not sufficient Sentinel-1A VH (vertically transmitted and horizontally received) backscatter observations to robustly evaluate DSSAT-MIMICS modeled VH performance. The sensitivity analyses revealed modeled backscatter was most responsive to wheat and rice stems, and corn leaves. Using the analyses, we developed a crop growth index that normalizes Sentinel-1A backscatter to modeled backscatter and mapped corn, rice, and wheat variability, identifying high and low crop growth in fields. This research contributes to the potential application of Sentinel-1A for crop monitoring. [DOI: 10.1117/1.JRS.14.044508]

Keywords: crop monitoring; Sentinel-1A; decision support system for agrotechnology transfer; Michigan microwave canopy scattering; synthetic aperture radar and modeling-based crop-index.

Paper 200497 received Jul. 1, 2020; accepted for publication Oct. 23, 2020; published online Nov. 12, 2020.

1 Introduction

Assessing crop and field conditions in a timely manner remains a challenge to agricultural management. This includes field conditions presowing, tracking growth stage and health, and within-field discrimination of crop development and stress. Accurate assessment of crop growth and field conditions can improve yield forecasts and enhance farm management practices.[1,2] Common monitoring efforts include field and airborne surveys, which can provide highly accurate measurements. However, field surveys can be difficult to perform over large areas and airborne surveys can be expensive and difficult to sustain throughout a growing season.[3]

Satellite-based remote sensing has the potential to improve the spatial and temporal scales of agricultural monitoring, essential to maintaining food production, and transform agricultural monitoring by enhancing large-scale understanding of crop dynamics across broad regional scales.[3] Optical/infrared (IR) remote sensing satellites are common choices to monitor agricultural fields but are limited to daytime and cloud-free conditions that can give rise to gaps in multitemporal monitoring.[4,5] Additionally, vegetation indices derived from optical/IR measurements, such as the normalized difference vegetation index, provide limited information on crop conditions.[6]

*Address all correspondence to Aaron Davitt, adavitt@gradcenter.cuny.edu

1931-3195/2020/$28.00

As an alternative, the availability of active microwave remote sensing datasets has significantly advanced with respect to the needs of agricultural monitoring owing to the launch of several space-based synthetic aperture radar (SAR) satellites. The advantages of SAR over optical/IR include independence from sunlight, thereby allowing for day and night coverage of the land surface throughout the year, in addition to "seeing" through cloudy conditions and atmospheric aerosols.[4,7,8] C-band (~5 GHz) SAR backscatter is sensitive to the entire crop canopy volume and to the moisture content of both the soil surface and canopy.[6,9] The launch of the C-band Sentinel-1A/B SARs has established a capability for routine, sustained monitoring of agricultural areas with SAR. This supports SAR monitoring of crops at spatial resolutions comparable to Landsat—tens of meters with weekly revisits.[10] The high temporal and spatial resolutions offered by SAR can identify crop growth cycles and generate within-field discrimination of growth during a growing season, providing a potentially valuable crop monitoring tool.[5,11]

The assessment of SAR backscatter sensitivity to various crops and to vegetation and surface moisture has been well documented. C-band SAR backscatter is sensitive to crop vegetation and growth, being dominated by vegetation when the leaf area index (LAI) is >0.5, with field geometry (i.e., row spacing and direction) having minimal impact on backscatter, especially at C-band and shorter wavelengths.[3,12,13] Ulaby and Bush[14] investigated the ability to monitor a corn field using a radar spectrometer, acquiring radar backscatter measurements in the range of 8 to 18 GHz. Their study demonstrated a strong correlation between radar and corn canopy water content. Previously published work has shown C-band radar backscatter to have a positive correlation with increasing LAI and a radar penetration depth limited to the upper canopy.[15–17] Furthermore, these studies revealed C-band radar backscatter is influenced by stages of corn development, with soil dominating the signal during juvenile corn growth and the canopy dominating during later stages of corn growth. In contrast, an inverse relationship occurs between backscatter and wheat growth—backscatter response decreases as wheat biomass increases.[9,18] For C-band radar, it was observed that the backscatter response decreased due to an increase in wheat biomass, and the VV-polarization (vertically transmitted and received) was more attenuated than HH-polarization (horizontally transmitted and received) owing to the vertical orientation of the wheat stems interacting more with VV-polarization.[19,20] Several studies[1,21–23] have shown the unique rice-radar signature interaction when monitored by satellite-borne C-band SARs (European Remote Sensing-1, Radarsat-1/2). As the rice stems emerge from a flooded field, there is a rapid increase in backscatter due to the increase radar interaction between the flooded surface and stems. The radar response tends to plateau when maximum rice biomass has been reached.

Radiometric models have been used to further our understanding of radar scattering from different crop canopies.[24–26] The Michigan microwave canopy scattering (MIMICS) model, a radar backscatter model based on radiative transfer theory, has been used to model the backscatter signature and variation from a walnut orchard, verified with scatterometer data.[24] Additionally, MIMICS has been applied to model backscatter for wheat, canola[25] and corn.[26,27] In these studies, MIMICS accurately modeled the radar backscatter variation, identifying scattering mechanisms contributing to total backscatter for each crop type and providing an understanding of the specific canopy moisture and structural features that influence the total measured radar signature. Della Vecchia et al.[9] conducted similar analyses for wheat and corn. Their model, Tor Vergata, captured the backscatter change, using *in-situ* corn and wheat field data during a growing season, and identified the dominant scattering mechanisms from the wheat fields. For rice, Le Toan et al.,[21] Koay et al.,[28] Oh et al.,[22] and Liu et al.[23] developed their own models to explain the radar scattering behavior from flooded rice fields, using *in-situ* ground data as inputs to their models. Oh et al. showed how backscatter increased during early rice growth, with a decrease in backscatter (attenuation) as the rice canopy matured. Liu et al. found rice stems were important scatterers, with radar responding more to stem attributes than other rice features.

While all of these studies further the understanding of SAR backscatter response from different crops, they have practical limitations with respect to agricultural monitoring. Many of these studies rely on field data to interpret SAR radar observations or as inputs to the radiometric models used. While field data are suitable for parameterizing and interpreting outputs from radiometric models, the collection of field data over larger spatial scales is difficult.

Additionally, radiometric models typically are applied to one crop type and management approach and use SAR backscatter as an evaluation of modeled backscatter results. The results from these models generally have not been used to inform on crop growth and conditions with SAR backscatter or to inform crop management practices. Finally, some of these studies that retrieve a specific crop parameter (e.g., LAI or biomass) do so by inverting the empirical relationship between the measured *in-situ* crop parameter and backscatter, making the inversion process site specific.[21,29,30] In all, these limitations prevent SAR application for agricultural monitoring in fields in different agricultural regions.

In this study, we evaluate an approach to assess variability in crop fields and growth for three staple crops—wheat, rice, and corn—using key surface and crop information from a dynamic crop growth simulation model [Decision Support System for Agrotechnology Transfer (DSSAT) Cropping Systems Model], instead of observations, for input to the MIMICS model. We compare MIMICS modeled backscatter to an ensemble mean Sentinel-1A backscatter from each crop field to understand Sentinel-1A backscatter variation from wheat, rice, and corn fields in Yolo County, California, for October 1, 2014, to September 30, 2015. Specifically, we:

1. Characterize the ability of the DSSAT and MIMICS combined architecture to model time-series Sentinel-1A radar backscatter response from wheat, rice, and corn fields.
2. Confirm backscatter sensitivity to wheat, rice, and corn canopy parameters, and ground surface parameters, as established in prior studies.
3. Create a crop growth index (CGI) value that assesses Sentinel-1A backscatter variability relative to a modeled reference backscatter to map Sentinel-1A backscatter variability in each crop field area.

The use of the DSSAT-MIMICS combination to provide an assessment of within-field variability has the potential to advance the application of SAR monitoring and assessment of crop development. By successfully linking remote sensing signatures to vegetation structure and moisture via this DSSAT-MIMICS approach, we contribute to the expansion of SAR-based agricultural assessments for improved crop monitoring, forecasting, and potential yield estimates in food-producing regions.

2 Methods

2.1 *Study Location*

Yolo County is situated in the Sacramento River Basin in the northern Central Valley of California (Fig. 1). This county is a well-studied, intensive agricultural region with crops covering 57% of the total land area (Fig. 1).[31] The climate of this area is defined as Mediterranean—cool, wet winters with hot and dry summers.[32] The cumulative sum for precipitation was 36.84 cm for water year 2015 (October 1, 2014, to September 30, 2015), based on Station 6 data from the California Irrigation Management Information System (CIMIS) near Davis, California. Precipitation fell mainly during the winter months, primarily in December 2014. Sporadic precipitation events occurred during the summer months with a cumulative total of 0.03 cm. Average air temperatures ranged from a minimum of 3.5°C (winter) to a maximum of 30.9°C (summer).

We focus our analyses on individual wheat, rice, and corn fields in Yolo County (Fig. 1). We selected 11 corn (11 acres, 4.45 ha) and 17 wheat fields (17 acres, 6.88 ha) located in the Russell Ranch Sustainable Agriculture Facility, operated by University of California, Davis.[33] Russell Ranch is an experimental farm where field conditions are monitored and controlled, supporting considerations for determining wheat and corn field conditions and the establishment of some crop management parameters in DSSAT. The fields we selected were fully watered, defined as either fully irrigated or as receiving irrigation supplemental to rain.

Rice fields in Yolo County were identified and selected using the U.S. Department of Agriculture National Agricultural Statistics Service (NASS) 2015 cropland data layer.[34] Once the rice fields were located with the cropland data layer, we used the unique radar backscatter response from rice fields during the early part of the growth phase,[21,23,28] a rapid increase in radar

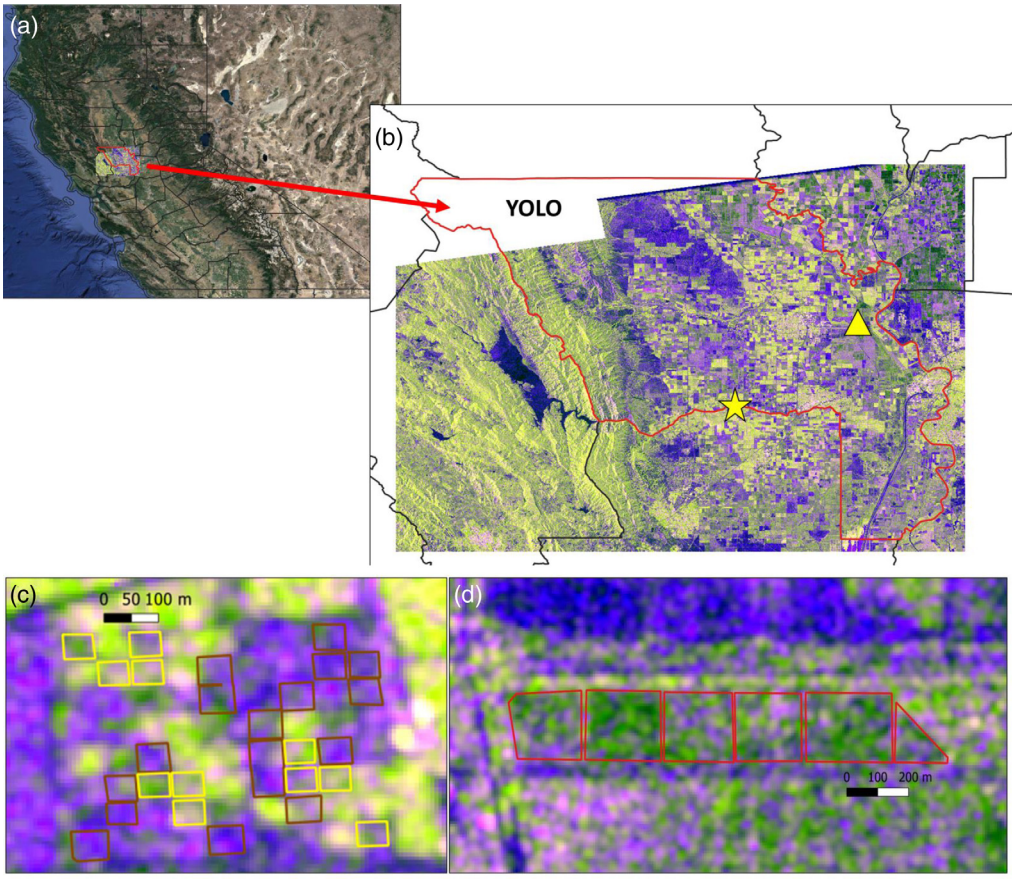

Fig. 1 (a) Location of Yolo County region (red outline) in the northern Central Valley of California. (b) Yolo County with Sentinel-1A false-color image ($R = \mathrm{VV}/G = \mathrm{VH}/B = \mathrm{VV}$; July 23, 2015) with crop fields marked—diamond marks wheat and corn fields at Russell Ranch and triangle marks rice fields. (c) Close-up of wheat (brown boxes) and corn (yellow boxes) fields at Russell Ranch. (d) Close-up of rice fields (red boxes) in eastern Yolo County.

Table 1 Summary of crop management parameters for DSSAT simulations.

Crop	Density (#/m^2)	Row spacing (cm)	Depth (cm)	Planting date	Harvest date
Corn	8	61	7	April 15, 2015	September 15, 2015
Rice	200	25	2.5	April 15, 2015	September 30, 2015
Wheat	270	16	3	November 15, 2014	March 30, 2015

backscatter as the rice stems emerge and elongate from a flooded field, to identify fields that were sowed and flooded in May 2015 and to set when rice is flooded for our crop management parameters in DSSAT (Table 1). In total, five rice fields (63 acres, 25.5 ha) were selected.

2.2 *SAR Data and Processing*

Sentinel-1A SAR operates at C-band ($\lambda = \sim$5.5 cm; 5.4 GHz), generating multitemporal dual-polarization (VV + VH; vertically transmitted and received, and vertically transmitted and horizontally received) backscatter measurements (σ^0_{VV} and σ^0_{VH}). Backscatter measurements are provided at 20-m resolution with a temporal revisit time of 12 days or less depending on the location.[35] Sentinel-1A interferometric wide swath level-1 ground range images were downloaded from the Alaska Satellite Facility Vertex.[36] Sentinel-1A images were selected based on

each crop's growing season defined by each crop's phenology and planting and harvest dates (Table 1).[37,38] For wheat, only single polarization (VV) was available during the growing season, so seven single-polarization (VV) images were used to observe growth. For corn, six single-polarization (VV) and four dual-polarization (VV + VH) images were used to observe growth. For rice, seven single-polarization and four dual-polarization images were used to observe growth.

The European Space Agency Sentinel Application Platform software was used to process the Sentinel-1A images, which included radiometric calibration and geocoding using the Doppler method that accounts for terrain correction.[39] Since the images were multi-looked and projected to ground range as part of this preprocessing, no additional speckle filter was applied, thus maintaining sufficient spatial resolution for our study. Multiple Sentinel-1A imagery from two orbit paths were included in the time-series assembly as each crop field was observed at similar incidence angles (42° to 44°).

Backscatter was generated for each crop in the following ways: (1) the mean field-level backscatter was generated for each field to support analysis of between-field backscatter variation. (2) The ensemble mean backscatter was determined for each crop type—wheat, rice, and corn—to support the DSSAT-MIMICS model analysis and assessment of the overall crop development and of the parameters that influence backscatter.

2.3 *DSSAT*

Crop parameters were estimated using the Crop Estimation through Resource and Environment Synthesis (CERES) component of DSSAT. DSSAT is a set of applications designed to understand, predict, and manage cropping systems at the field scale.[40,41] DSSAT runs on a daily time step with crop yield estimates dependent on surface meteorology, a detailed soil profile, cultivar genetics, and management. DSSAT simulates biological processes that track carbon, nitrogen, water, and energy budgets, and associated stresses, through a crop's developmental stages as it interacts with the environment and agricultural management practices. DSSAT supports models for 27 unique crop species, including all the major staple crops, and has been used in agricultural systems around the world for a variety of applications.[42–46] In our simulations, we run the CERES-Maize, CERES-Wheat, and CERES-Rice applications of DSSAT, which have been widely used in crop modeling and studies of California's Central Valley.[47–49]

DSSAT was run for the 2015 water year, initializing October 1, 2014, and ending September 30, 2015. DSSAT was driven with surface (2 m) maximum and minimum air temperature, precipitation, surface wind speed, surface relative humidity, and insolation from Station 6 of the Station CIMIS, located in Davis, California.[50] DSSAT has primarily been used for staple crops, so our initial assessment of climate impacts on irrigated agriculture is focused on corn (maize; *Zea mays*), winter wheat (*Triticum aestivum*), and rice (*Oryza sativa*). Crop management information is described in Table 1.

Planting dates are consistent with the crop phenology and typical planting dates in the region and are accurate in all but exceptional circumstances.[37,38] Soil properties, including soil moisture initialization, were defined for all crops using a generic deep sandy loam profile. Details on the construction and attributes of the soil profile are included in the DSSAT source code.[40] According to Russell Ranch field information, wheat and corn crops were well fertilized, so we turned off nutrient stress in DSSAT for both crops. We also assumed no nutrient stress for rice. Automatic irrigation for corn and wheat is triggered when the fraction of soil moisture in the top 30 cm of the soil profile falls below 50% of soil saturation. Water is then applied as furrow irrigation until the soil moisture level reaches 100% saturated. Rice is flooded on May 1, 2015, through harvest to a depth of 100 mm. Bund height is set to 150 mm, and percolation rate is assumed to be 4 mm day^{-1}. Simulations for each crop type were run using the observed atmospheric CO_2 concentration time series.[51]

Crop varieties were selected for each of the three crops based on the field and management characteristics of Yolo County. Growers in this area generally use slow-maturing corn varieties to take advantage of the long growing season in the region.[37,52] We selected a corn cultivar in DSSAT that contains the generic attributes of California corn but does not match a specific variety grown in Yolo County both because the corn variety grown at Russell Ranch is not

available in DSSAT and because we seek to maintain flexibility for model applications beyond Yolo County. Most of California's wheat production is hard red spring wheat planted in the fall (University of California Division of Agriculture and Natural Resources, 2006). Important characteristics for California wheat production include short stature, lodging resistance, soil saturation tolerance, shatter resistance, and nitrogen responsiveness (University of California Division of Agriculture and Natural Resources[53]). A hard-red spring wheat cultivar with the desired properties was not available in DSSAT, so a hard-red winter wheat available in DSSAT was selected. Rice production in California is dominated by semidwarf, medium-grain varieties, with the majority classified as early maturity.[54,55] These varieties provide a high yield and quality of rice and flexibility in planting dates due to the relatively short time to maturity. As with corn, a rice cultivar in DSSAT was selected that contains the key properties of rice currently grown in California because an exact match for the rice field trial variety was not available in DSSAT and to ensure that the model is valid for applications throughout California.

Not all crop structure parameters are provided by DSSAT (e.g., wheat ears and rice panicles). However, DSSAT does provide the key time-evolving biophysical parameters that describe each crop's growth. For wheat and rice, DSSAT provides tiller density, a critical biophysical parameter of wheat and rice growth, and yield determination.[55–57] For corn, DSSAT provides numerous key biophysical parameters of corn growth, including leaf diameter (derived from LAI) and stem density (Table 2). While DSSAT output parameters are generated at the point-scale level, and therefore, do not necessarily represent all the variation that can occur within individual wheat, rice, and corn fields, DSSAT provides a reasonable average set of parameters and conditions by crop type based on a specific planting date and set of management practices. We use these parameters as inputs to MIMICS to support understanding backscatter response to surface and crop conditions.

2.4 *Radiometric Modeling*

Microwave radar backscatter from wheat, rice, and corn canopies was simulated using the MIMICS model. MIMICS is a fully polarimetric radar scattering model based on radiative transfer theory and has been used to evaluate radar backscatter sensitivity to crop and surface structure, and moisture features (i.e., vegetation canopy structure and moisture, and soil moisture; McDonald et al.; and Frolking et al.). MIMICS models a vegetation canopy as a layer of discrete scattering constituents on top of a semi-infinite rough ground surface. The model supports a physically based understanding of the behavior of microwave energy propagating through a vegetation medium. While MIMICS was developed to model backscatter from tree canopies as either a two or three-layer model, the model is adaptable for a variety of vegetation canopies, including crops.[4,24–26] Detailed information on MIMICS can be found in Ref. 24.

We use MIMICS with input parameters provided by DSSAT output to examine the scattering mechanisms contributing to the backscatter measurement and the sensitivity response to each crop parameter modeled. This allows us to link the vegetation and surface properties to backscatter signatures and provide a backscatter reference for crop growth to compare with Sentinel-1A observations.

3 Methods

3.1 *Informing MIMICS with DSSAT*

The flow chart in Fig. 2 shows the overall methodology employed in this study. Local CIMIS meteorological data and initial management conditions were used to force DSSAT to generate surface and crop parameters for wheat, rice, and corn. DSSAT provided the key time-evolving biophysical inputs to represent crop growth. Parameters not provided by DSSAT, but needed in the radiometric modeling, were derived from previously published research. Table 2 describes the parameters used in MIMICS, listing those provided by DSSAT and those supplemented from prior research, and the equivalent MIMICS input.

Table 2 Crop parameters, source, and MIMICS input to model backscatter for wheat, rice, and corn canopy.

Crop	Parameter	Source	MIMICS input
Wheat	Tiller density (#/m^2)	From DSSAT	Needle density
	Height (m)	Function from Toure et al. 1994	Canopy height and needle length
	Stem orientation*	From Toure et al. 1994	Needle orientation
	Stem diameter*	Mean, from various sources	Needle diameter
	Soil Moisture (cm^3/cm^3)	From DSSAT	Soil volumetric moisture content
	rms and correlation length (cm)*	From Toure et al. 1994	rms and correlation length
Rice	Tiller density (#/m^2)	From DSSAT	Needle density
	Height (m)	Function from Oh et al. 2009	Canopy height and needle length
	Stem orientation*	From Koay et al. 2007	Needle orientation
	Stem diameter*	Mean from various sources, in text	Needle diameter
	rms and correlation length (cm)*	From Koay et al. 2007	rms and correlation length
Corn	Stem density (#/m^2)*	From DSSAT	Canopy density
	Stem orientation*	From McDonald 1991	Trunk orientation
	Stem diameter	From Della Vecchia et al. 2006	Trunk diameter
	Height (m)	From DSSAT	Canopy and trunk height
	Leaf density (#/m^2)	From DSSAT	Leaf density
	Leaf diameter (cm; from LAI)	From DSSAT	Leaf diameter
	Leaf orientation*	From McDonald 1991	Leaf orientation
	Leaf thickness (cm)*	From McDonald 1991	Leaf diameter
	Soil moisture (cm^3/cm^3)	Form DSSAT	Soil volumetric moisture content
	rms and correlation length (cm)*	From McDonald 1991	rms and correlation length

Asterisk symbols indicate parameters modeled as constants in MIMICS.

MIMICS was parameterized independently for each crop. Wheat was modeled as in Ref. 25—a single vegetation layer canopy consisting of dielectric cylinders with vertical orientation over a rough ground surface. For rice, a similar set up to Ref. 28 was used—a single vegetation layer consisting of dielectric cylinders with vertical orientation over a rough water surface. For wheat and rice, no trunk and leaf inputs were used and associated parameters were omitted. Tiller density (hereafter referred to as stem density) is considered a primary indicator of wheat and rice health and grain yield and DSSAT provides this primary indicator.[53,56,58]

Corn was modeled as two layers of vegetation consisting of stalks and leaves over a rough ground surface.[27] Corn stalks were modeled as dielectric cylinders and leaves were modeled as oblate dielectric spheroids (oblate disks).

All MIMICS simulations employed the UMich Empirical developed by Oh et al. to model backscatter from the ground.[59] This model is fully integrated within the MIMICS architecture, has been verified across a broad range of surface roughness and soil moisture conditions, and can model both co- and cross-polarization backscatter.[59–61] The UMich Empirical model was set to

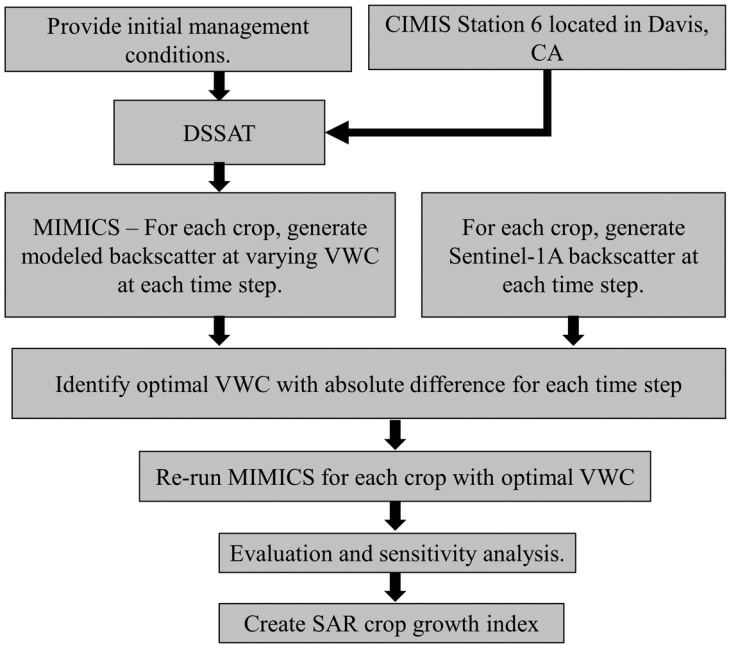

Fig. 2 Flowchart depicting the approach that uses DSSAT, MIMICS, and Sentinel-1A to describe field variability. Approach description is provided in text.

the Sentinel-1A frequency (5.4 GHz) and acquisition incidence angle (43°) based on the crop fields' locations. The model used for vegetation dielectric constant is the Debye–Cole dual-dispersion model that incorporates the vegetation gravimetric moisture content.[62] The model used for soil dielectric constant is the empirical model developed by Ref. 63.

A time-series dataset of soil surface and crop parameter inputs were used to drive MIMICS. For each crop, the parameters in Table 2 were matched to Sentinel-1A acquisition dates in water year 2015 (e.g., Julian day 144 in DSSAT corresponds to Sentinel-1A acquisition on May 24, 2015) and adapted as input to MIMICS. Wheat and rice stem diameters were modeled as constant with a mean value created from various sources.[9,23,25] Stem and leaf moisture content were not modeled in DSSAT, and field measurements of time-evolving plant moisture content are not common. These parameters, however, are required for MIMICS and associated interpretation of radar backscatter. To address this, we used an iterative approach that models backscatter values for a range of observed gravimetric moisture contents [g/g, hereafter, referred to as vegetation water content (VWC)]. First, the range of observed VWCs for each crop type were set in MIMICS at each time step.[7,21,23,25,64] Corn leaf VWCs were given slightly lower values compared to the corn stems, as described in Ref. 64. Once the model generated a range of backscatter values at different VWCs for each time step, we retrieved the optimal VWC by finding the smallest absolute difference between MIMICS and Sentinel-1A σ^0_{VV} in linear units

$$\text{Optimal VWC}_t = |M\sigma^0_{\mathrm{VV}t} - \mathrm{S1A}\sigma^0_{\mathrm{VV}t}|. \tag{1}$$

If a time step had observed both σ^0_{VV} and σ^0_{VH}, then the following was used

$$\text{Optimal VWC}_t = ||\mathrm{M}\sigma^0_{\mathrm{VV}t} - \mathrm{S1A}\sigma^0_{\mathrm{VV}t}| - |\mathrm{M}\sigma^0_{\mathrm{VH}t} - \mathrm{S1A}\sigma^0_{\mathrm{VH}t}||, \tag{2}$$

where $M\sigma^0_{\mathrm{VV}}$ and $M\sigma^0_{\mathrm{VH}}$ are MIMICS modeled backscatter by polarization, $\mathrm{S1\,A}\sigma^0_{\mathrm{VV}}$ and $\mathrm{S1\,A}\sigma^0_{\mathrm{VH}}$ are Sentinel-1A backscatter by polarization, and t is the time step. We used only the mean ensemble Sentinel-1A σ^0_{VV} and σ^0_{VH} from each crop to provide a frame of reference to constrain the VWCs to identify the optimal value to model backscatter for each crop.

3.2 *Evaluation of Approach*

The optimally retrieved VWC for each crop's time step was combined with the previous crop parameters and MIMICS was rerun with these updated inputs. This created the modeled backscatter time series needed to assess the approach for identifying the scattering components and backscatter response to the appropriate crop parameters. We calculated Esys (systematic error or model bias), root-mean-squared error (RMSE), and Pearson correlation coefficient (Rp) between the MIMICS modeled and ensemble mean Sentinel-1A backscatter time series. Additionally, we assessed the MIMICS modeled backscatter scattering contributions to total backscatter to identify those canopy constituents (e.g., the crop canopy or soil moisture) that were dominant in the total radar backscatter (Fig. 3). For example, as a corn grows, the density of radar scatterers in the vegetation canopy increases. Correspondingly, the dominant radar scattering process transitions from one involving soil backscatter to one dominated by scattering from the vegetation components.[6]

A sensitivity analysis was performed to understand how different crop and soil surface parameters influenced backscatter. For each crop type, crop vegetation and surface parameters, and the optimally retrieved VWCs, used to create the MIMICS σ^0_{VV} time-series, were varied by $\pm 10\%$ to examine the radar response

$$\Delta \mathrm{dB} = 10 * \mathrm{Log10}(\mathrm{MIMICS}\,\sigma^0_{VV}/\mathrm{MIMICS\ varied}\,\sigma^0_{VV}), \tag{3}$$

where MIMICS σ^0_{VV} is the modeled backscatter value from the original time-series model run, and MIMICS varied σ^0_{VV} is the modeled backscatter value with the input parameter varied by $\pm 10\%$ from the original time-series model run. The $\pm 10\%$ was selected based on previous work understanding how DSSAT cultivar parameters influence yields and how modeled backscatter responds to individual crop parameters.[23,31]

The sensitivity analysis was performed on each parameter and on multiple parameters that are intrinsically linked, e.g., wheat and rice stem heights and diameters, and corn leaf diameter and thickness. This supports understanding how individual parameters and combinations influence radar response. This sensitivity analysis provided valuable information about the suitability of the optimization approach applied using DSSAT-MIMICS and how backscatter responds to each parameter through the growing season. Use of σ^0_{VV} was emphasized for the sensitivity analysis since σ^0_{VH} measurements were unavailable for wheat and sparse for rice and corn.

3.3 *Crop Growth Index*

A challenge for crop monitoring and describing within- and between-field variability is providing an indicator representing a specific set of crop growth conditions. We examined the potential for SAR to address these challenges by developing a SAR CGI that could provide the basis for

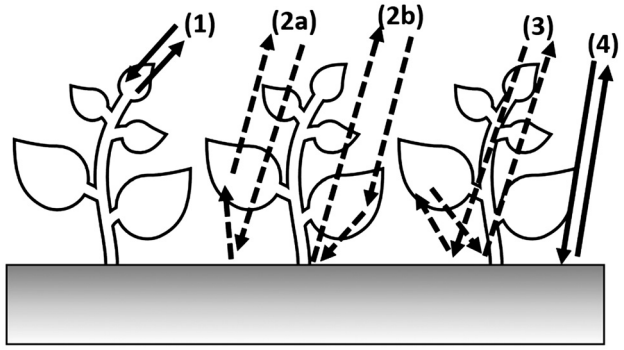

Fig. 3 Illustration of scattering mechanisms from a crop canopy and underlying surface—(1) Scattering from canopy (direct canopy); (2a) Scattering from the soil and canopy (ground-canopy), and (2b) the reciprocal process to (2a) (canopy-ground); (3) Multiple scattering from the soil, canopy, and soil (ground-canopy-ground); (4) Scattering from soil (direct ground). The reciprocal terms (2a) and (2b) are combined as one term, hereafter referred to as canopy-ground.

in-season near-real-time crop monitoring. SAR CGI is an extension of the sensitivity analysis where we compare each within-field Sentinel-1A backscatter value to a DSSAT-MIMICS modeled backscatter value. To map SAR CGI, dates when DSSAT-MIMICS backscatter best matches the ensemble mean Sentinel-1A backscatter per crop were used. Then the difference between each within-field Sentinel-1A σ^0_{VV} pixel and DSSAT-MIMICS modeled σ^0_{VV}, was performed

$$\text{SAR CGI(dB)} = 10 * \text{Log}\,10(\text{S1A}\,\sigma^0_{VV,t,i}/\text{DM}\,\sigma^0_{VV,t}), \tag{4}$$

where DM $\sigma^0_{VV,t}$ is DSSAT-MIMICS modeled backscatter for VV-polarization at time "t" with t being the specific date [expressed in days after planting (DAP)], and S1A $\sigma^0_{VV,t,i}$ is Sentinel-1A backscatter at time t for the individual area "i" (pixel) in the crop field. To account for the inverse relationship between radar response for wheat (see Sec. 5, wheat sensitivity analysis), a factor of -1 is introduced. A comparison of Sentinel-1A σ^0_{VH} and DSSAT-MIMICS modeled σ^0_{VH} was not used due to the lack of sufficient cross-polarized data for corn and rice, and absence of data for wheat.

The SAR CGI describes relative crop growth by quantifying the difference between Sentinel-1A backscatter and DSSAT-MIMICS modeled backscatter, the latter being the reference backscatter for a field developing under nonstressed growth conditions. Thus, a negative (positive) SAR CGI represents areas of less (more) crop growth as measured by Sentinel-1A relative to growth modeled by the DSSAT-MIMICS construct. This provides a flexible indicator to understand within- and between-field variability without the site-specific retrieval of crop conditions used in previous studies. We focus on two dates when DSSAT-MIMICS and Sentinel-1A backscatter were similar for each crop, one during early and one during late crop growth stages, for application of SAR CGI.

4 Results

The results of the wheat, rice, and corn field variability as observed by Sentinel-1A, DSSAT-MIMICS modeled performance, sensitivity analysis, and SAR CGI are presented. We use the matching DAP provided by DSSAT for interpreting the Sentinel-1A (hereafter, S1) and DSSAT-MIMICS modeled backscatter signatures. Inputs parameters used in MIMICS are provided to describe wheat, rice, and corn growth and backscatter change.

4.1 *Sentinel-1A Wheat, Rice, and Corn Fields Backscatter*

Wheat fields display a decreasing S1 σ^0_{VV} for the growing season (Fig. 4). This is similar to other studies that show a decreasing σ^0_{VV} as the wheat canopy develops.[19,20] Additionally, each of the fields' mean field backscatter time series suggests differing amounts of wheat vegetation and development throughout the growing season. On 94 DAP, there is an increase in σ^0_{VV}, which may be caused by irrigation, as the CIMIS data indicate no preciptation in the prior days and weeks.

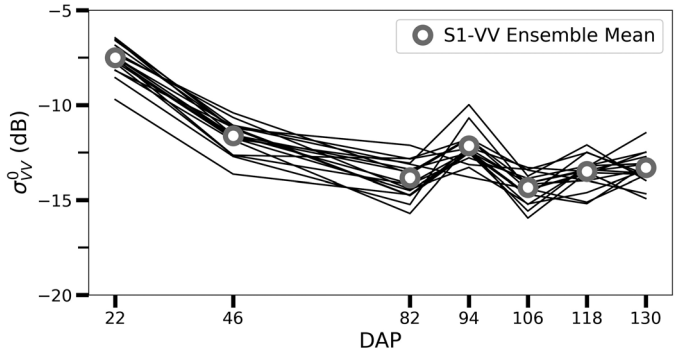

Fig. 4 Wheat fields mean Sentinel-1A σ^0_{VV}. Each line indicates individual wheat fields with S1-VV ensemble mean (gray open-circle markers).

After 94 DAP, there is an increasing trend in σ^0_{VV}, which is associated with wheat thinning and drying, allowing σ^0_{VV} to interact more with the ground.[19,20]

The rice fields display similar S1 σ^0_{VV} temporal variation with each other, a rapid backscatter increase that can be associated with stem elongation during the initial growth stages (Fig. 5).[1,21–23] Before 75 DAP, the rice fields display a larger dynamic range, suggesting that some fields may have experienced delayed growth. After 75 DAP, the range decreases and all the fields have similar σ^0_{VV} variation, which increases toward harvest. Each of the rice fields' mean backscatter time series suggests varying rice canopy development through the growing season. Only a few dates of S1 σ^0_{VH} are available and follow σ^0_{VV}, where backscatter increases as the rice canopy develops.

Corn fields display a greater dynamic range compared to wheat and rice, with as much as a 4-dB range difference on different DAPs (Fig. 6). No single field maintains a consistenly high or low backscatter signature, suggesting varying rates of corn canopy development. All fields selected are fully irrigated. The field-to-field variability in backscatter suggests an increased sensitivity to corn vegetation volume and structure between the fields. Corn exhibits more field-to-field variability than do wheat and rice fields, especially as related to the geometry of the leaves. This backscatter response shares similarities to SAR scattering from corn canopies of different structural attributes.[6] The ensemble mean S1 σ^0_{VV} increases after 39 DAP, which stablizes and decreases toward harvest after 123 DAP. The few avaliable S1 σ^0_{VH} have a similar response, backscatter increases during the corn growing season and decreases toward harvest. This S1 σ^0_{VV} and σ^0_{VH} temporal change are similar to others SAR studies of corn.[15,16]

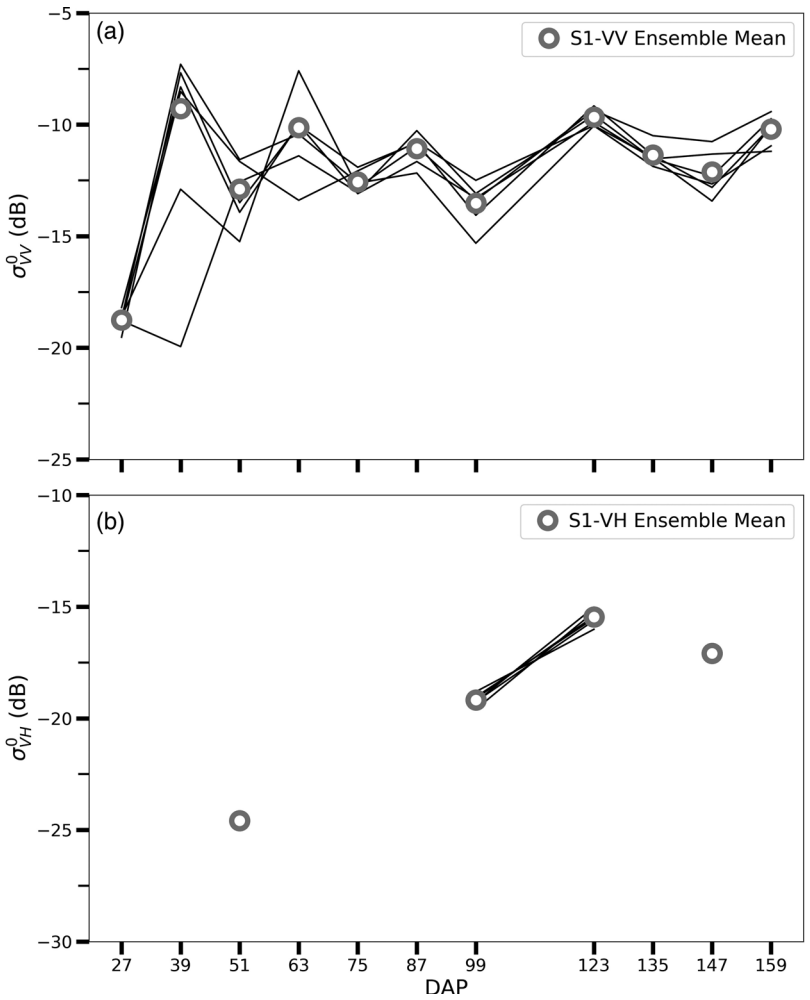

Fig. 5 (a) Rice fields mean Sentinel-1A σ^0_{VV} and (b) mean Sentinel-1A σ^0_{VH}. Each line indicates individual rice fields with S1-VV and VH ensemble mean (gray open-circle markers).

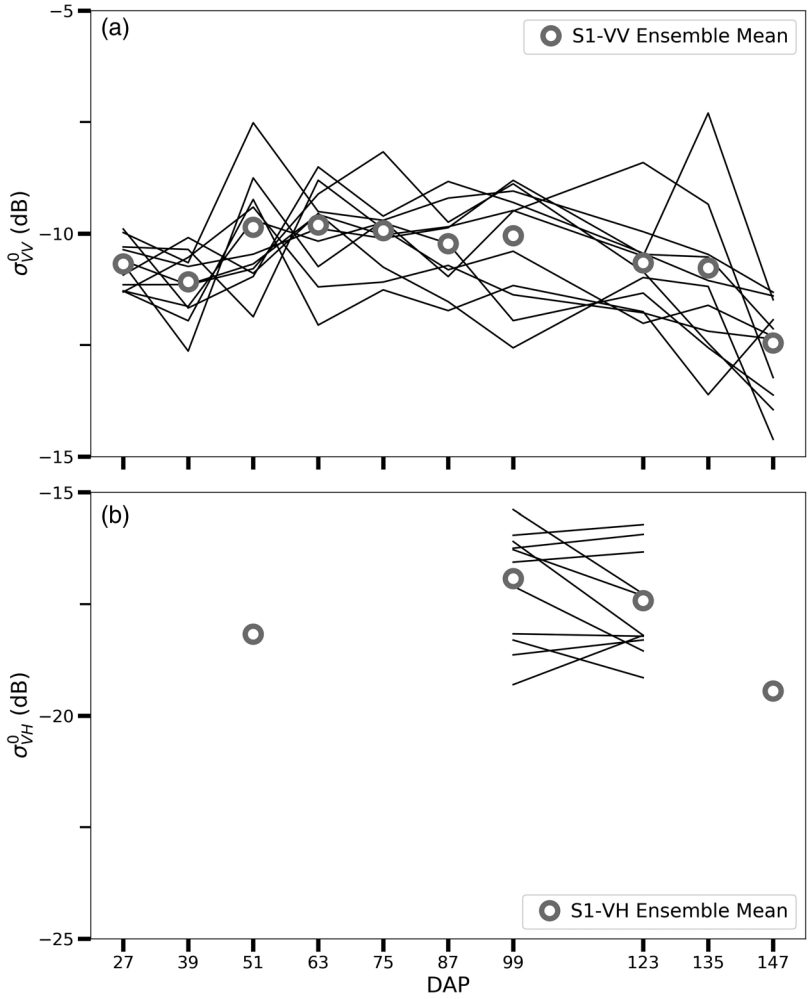

Fig. 6 (a) Corn fields mean Sentinel-1A σ^0_{VV} and (b) mean Sentinel-1A σ^0_{VH}. Each line indicates individual corn fields with S1-VV and VH ensemble mean (gray open-circle markers).

4.2 *MIMICS-Modeled Backscatter Response and Model Performance*

MIMICS modeled σ^0_{VV}, associated scattering contributions, and ensemble mean S1 σ^0_{VV} for the wheat fields are shown in Fig. 7. S1 cross-polarization was not available during the wheat growing season. The modeled backscatter reproduces the S1 σ^0_{VV} decrease that is associated with radar signal attenuation as the wheat canopy develops ($Rp = 0.84$, $p < .05$, RMSE = 1.55 dB, and Esys = .99 dB). The DSSAT-MIMICS approach underestimates S1 backscatter before 82 DAP, ranging between 0.1 and 2.9 dB. These DAPs are associated with juvenile wheat canopy growth, as the stem density and canopy height increases. On 94 DAP, MIMICS modeled backscatter does not capture the observed S1 σ^0_{VV} increase, indicating a change of field condition that DSSAT did not capture. Later in the wheat growing season (106, 118, and 130 DAPs), the MIMICS modeled backscatter matches the increasing S1 backscatter, when the wheat stem density thinned and decreased in height.

The direct ground scattering contribution is the largest single contributor to MIMICS total backscatter (σ^0_{VV}) for wheat. For the entire wheat growing season, the ground contribution is similar to total backscatter and S1 σ^0_{VV} variability (Fig. 7). Other contributors, such as direct canopy scattering, were relatively negligible in contribution to the total backscatter signature.

Retrieved wheat stem VWCs fall within wheat moisture values previously reported by Ref. 25 and show minimal variation during the wheat growing season. Stem VWC remains at 0.48 on 94 DAP, just after max tiller density. Afterward, stem VWC increases to 0.53, then reduces to 0.48 on 130 DAP, at harvest. The relative lack of change in stem VWCs can be

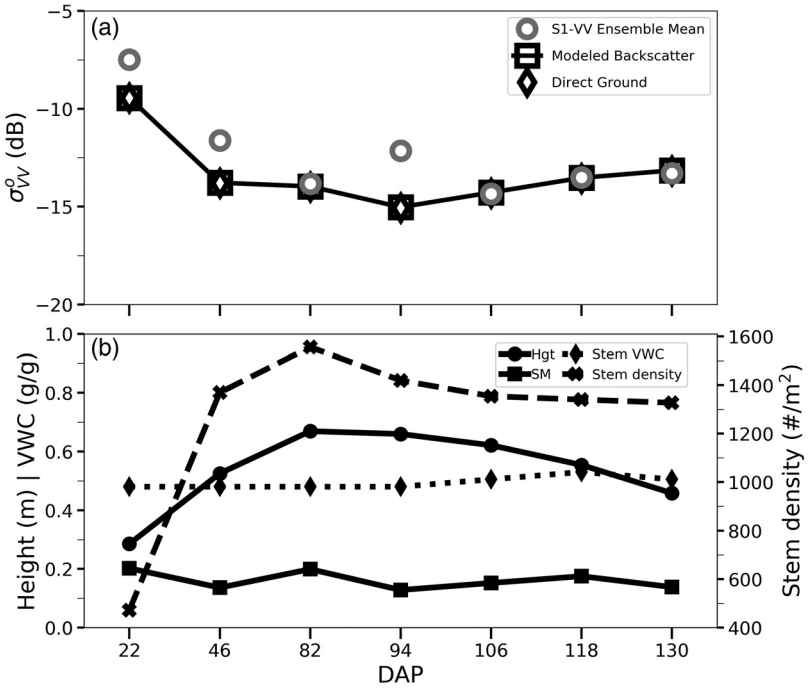

Fig. 7 (a) Wheat S1-VV ensemble mean (open circles) and MIMICS modeled (open square-line) σ^0_{VV} (dB) with the major contributor to modeled backscatter (direct ground and diamond-dashed line). Scattering mechanisms < – 20 dB not shown. (b) Retrieved VWC (stem VWC, diamond-dashed line) and parameters used to model backscatter—height (Hgt, circle line); soil moisture (SM, square line); Stem density (X-dashed line).

attributed to the dominance of the direct ground scattering contribution to the total backscatter signal. While the wheat canopy can attenuate radar response, the surface provides the magnitude for the total modeled backscatter signature.

MIMICS modeled and ensemble mean S1 σ^0_{VV} and σ^0_{VH} for rice are shown in Fig. 8. MIMICS σ^0_{VV} compares well to S1 σ^0_{VV} (Rp = 0.81, $p < .05$, RMSE = 1.62 dB, and Esys = −0.07 dB). The DSSAT-MIMICS approach reproduces the S1 σ^0_{VV} on 27 and 39 DAP, where the difference between modeled and S1 backscatter was 0.05 and 0.46 dB, respectively. These two DAPs coincide with increasing stem density and height. MIMICS modeled σ^0_{VV} is greater and less than S1 σ^0_{VV} on 51 and 87 DAP, respectively, but matches on 63, 75, and 99 DAP. On these DAPs, the rice canopy reaches maximum stem density and height. After 99 DAP, stem density decreases and MIMICS modeled and S1 σ^0_{VV} are similar on 135 and 159 DAP (0.20 and 0.04 dB for each) but modeled σ^0_{VV} overpredicts on 147 DAP by 3.9 dB.

MIMICS modeled σ^0_{VH} generally reproduces the increasing backscatter from the rice fields but, based on the few S1 cross-polarization dates available, the model underperforms compared to the copolarization ($Rp = 0.39$, $p = .61$, RMSE = 3.93 dB, Esys = 2.22 dB). MIMICS modeled and S1 σ^0_{VH} increases in response to the growing rice canopy. Modeled σ^0_{VH} is slightly higher and lower than S1 on 51 and 99 DAP, respectively. Modeled σ^0_{VH} underpredicts S1 σ^0_{VH} by 7.5 dB on 123 DAP and is similar to S1 σ^0_{VH} on 147 DAP.

MIMICS modeled σ^0_{VV} and σ^0_{VH} are dominated by the canopy-ground scattering contribution, representing the double-bounce scattering interaction between the rice canopy and water surface. The canopy-ground scattering contributor follows the MIMICS modeled backscatter change and is similar to S1 backscatter. The main contributor suggests that backscatter from a rice field, modeled or observed, is strongly influenced by the double-bounce scattering between the rice stems and flooded surface.

Retrieved stem VWCs fall within previously reported measured values and follow changes in rice vegetation moisture—an overall decrease in moisture content as the rice canopy matures.[65,66] VWC decreases after 39 DAP from 0.90 and varies around 0.60. Toward harvest, the retrieved values increase to 0.80, and subsequently decrease to 0.63. This increase can be attributed to the

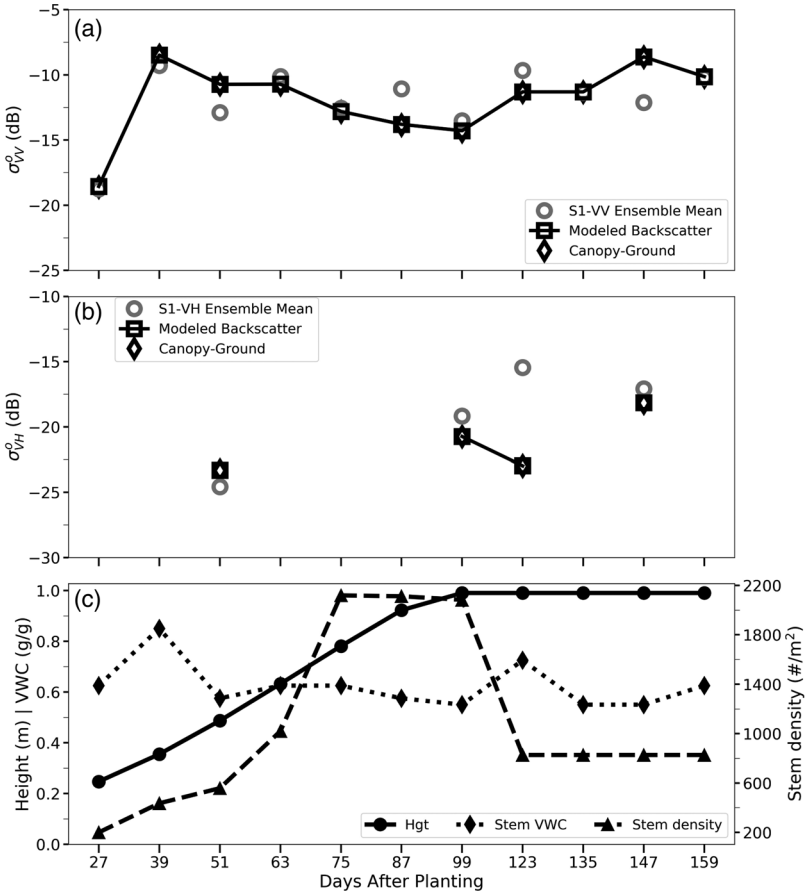

Fig. 8 (a) Rice S1-VV ensemble mean (open circles) and MIMICS modeled (open square-line) σ^0_{VV} (dB) with major contributors to model backscatter (canopy-ground, diamond-dashed line). Scattering contributions < -25 dB not shown. (b) Rice S1-VH ensemble mean (open circles) and modeled (open square-line) σ^0_{VH} (dB) from rice fields with major contributors to model backscatter (canopy-ground, diamond-dashed line). Any contributions < -30 dB were considered negligible. (c) Retrieved VWC (Stem VWC, diamond-dashed line) and parameters used to model backscatter—height (Hgt, circle line); Stem density (triangle-dashed line).

input parameters used in MIMICS on this DAP. Since the VWC is found with a set of rice stem input parameters, this creates the unusually high VWC to match MIMICS modeled backscatter to Sentinel-1A. This suggests the stem height and/or density inputs on 147 DAP may need to be lower to represent what S1 was observing in the rice fields.

Corn canopy MIMICS modeled backscatter, scattering contributions, and ensemble mean S1 σ^0_{VV} and σ^0_{VH} are shown in Fig. 9. The DSSAT-MIMICS combination models a backscatter response similar to S1 σ^0_{VV} ($Rp = 0.64$, $p < .05$, RMSE $= 0.97$ dB, and Esys $= -0.23$ dB). The low Rp value is due to correlation sensitivity to outliers, the 3 dB mismatch on 27 DAP. When Rp is performed excluding 27 DAP, Rp increases to 0.95 ($p < 0.01$). This mismatch on DAP 27 suggests that the inputs used in MIMICS may reflect a less-developed corn canopy than what actually existed, and hence, a more developed canopy structure actually existed. From 39 to 87 DAP, modeled and S1 σ^0_{VV} are similar, with a difference of ~0.15 dB. This time range corresponds to increasing corn height and LAI growth. After 87 DAP, MIMICS modeled and S1 backscatter decreases as corn LAI decreases; modeled backscatter differs from S1 σ^0_{VV} by 0.10 to 0.5 dB. For the few available S1 σ^0_{VH} measurements, DSSAT-MIMICS σ^0_{VH} captures the backscatter increases and decreases seen with S1 σ^0_{VH}, which can be in response to changing LAI ($Rp = 0.63$, $p = 0.37$, RMSE $= 2.69$ dB, and Esys $= 2.43$ dB). MIMICS modeled σ^0_{VH} underpredicts S1 backscatter for the available acquisitions by 0.50 to 3.7 dB on 51, 99, 123, and 147 DAP.

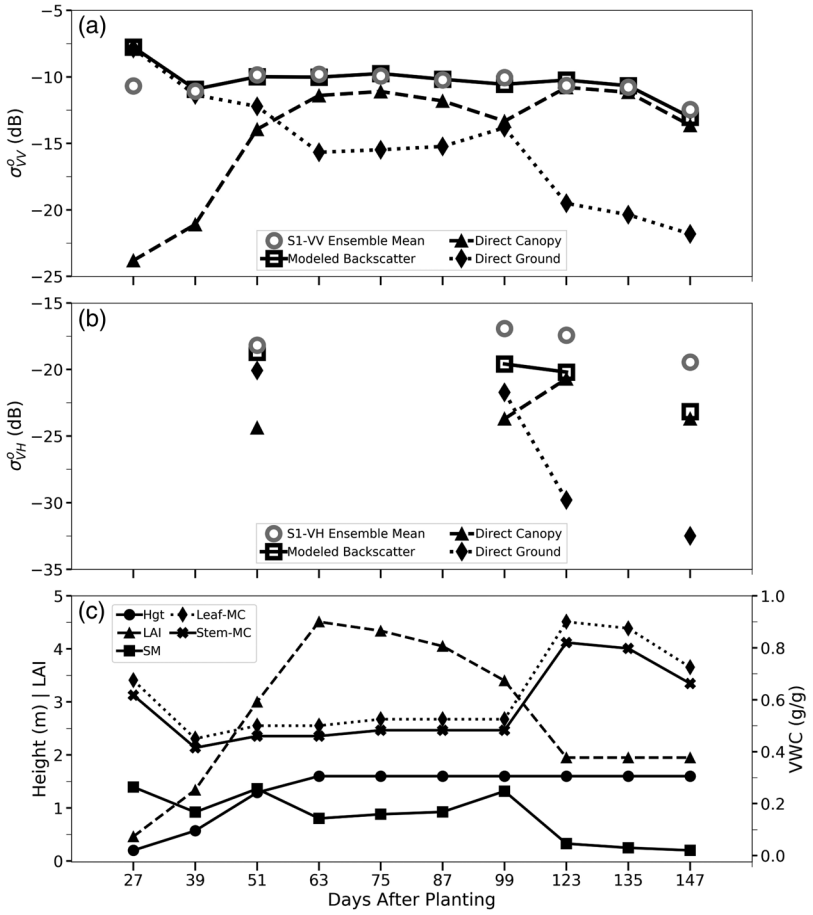

Fig. 9 (a) Corn S1-VV ensemble mean (open circles) and MIMICS modeled (open square-line) σ^0_{VV} (dB) with major contributors to model backscatter (direct canopy and triangle-dashed line; direct ground and diamond-dashed line). Scattering contributions < – 25 dB not shown. (b) Corn S1-VH ensemble mean (open circles) and modeled (square-line) σ^0_{VH} (dB) with major contributors to model backscatter (direct canopy and triangle-dashed line; direct ground and diamond-dashed line). Scattering contributions < – 35 dB not shown. (c) Retrieved VWC (leaf VWC, diamond-dashed line; stem VWC, *x*-line) and parameters used to model backscatter—height (Hgt, circle line); LAI (triangle-dashed line); soil moisture (SM, square-line).

The contributors to MIMICS modeled σ^0_{VV} and σ^0_{VH} vary. Direct ground scattering dominates the total backscatter signal up to 51 DAP and switches to direct canopy scattering. The direct ground contribution diminishes as the canopy develops after 51 DAP. On 99 DAP, there is an increase in direct ground contribution, associated with a higher soil moisture value and lower corn LAI. The direct ground contribution is more apparent for σ^0_{VH} on 99 DAP. Overall, this suggests the contribution to total backscatter is initially driven by the surface and minimally by the juvenile corn canopy. As the corn canopy develops, the situation transitions to the scattering dominated by a mature corn canopy.

The retrieved corn stem and leaf VWCs fall within previously measured values for corn.[64] The retrieved stem and leaves VWC decrease from 0.68 and 0.62 (27 DAP) and varies between 0.45 and 0.53 up to 99 DAP. The VWC decrease may be due to ground contribution influencing total backscatter measurement, making the retrieval of VWC for early corn growth challenging. The minimal variation up to 99 DAP is not unusual as corn stem and leaf VWCs can remain relatively stable for certain periods during the growing season.[67] Additionally, the lower VWC values suggest the corn leaf geometry influence backscatter the most. The combined MIMICS-DSSAT approach retrieves higher stem and leaf VWC, up to 0.90, on 123 and 135 DAP, and a reasonable value on 147 DAP. While it has been reported that corn canopies experience some reduction in moisture during the growth season, it has been reported that corn leaf and stem

VWCs can remain relatively high toward harvest; or the LAI may need to be higher to represent what S1 was observing in the corn fields.[64,67]

5 Sensitivity Analysis

We explore how crop and ground surface parameters influence σ^0_{VV} through a sensitivity analysis. For each crop, all the parameters and the retrieved VWCs used to create a MIMICS σ^0_{VV} in Figs. 7 to 9 were varied by $\pm 10\%$ to examine the radar response. Figures 10 to 12 show how some of these individual parameters and combinations can vary radar response through the growing season.

Regardless of crop type, the vegetation parameters influence radar backscatter to a higher degree than surface parameters, either separately or in combination (Table 3). Wheat and rice stem height, diameter, and density produced the largest response, close to 2 and 1.7 dB, respectively. Closer examination shows that wheat and rice stem height and diameter are the primary parameters with stem density having a smaller radar response. Corn leaf diameter, thickness, and density produce the largest radar response, 1.63 dB. Closer examination shows the leaf diameter influencing the radar response the most, with leaf thickness and density having a smaller influence on radar response. For corn and wheat, soil moisture and roughness are up to four times

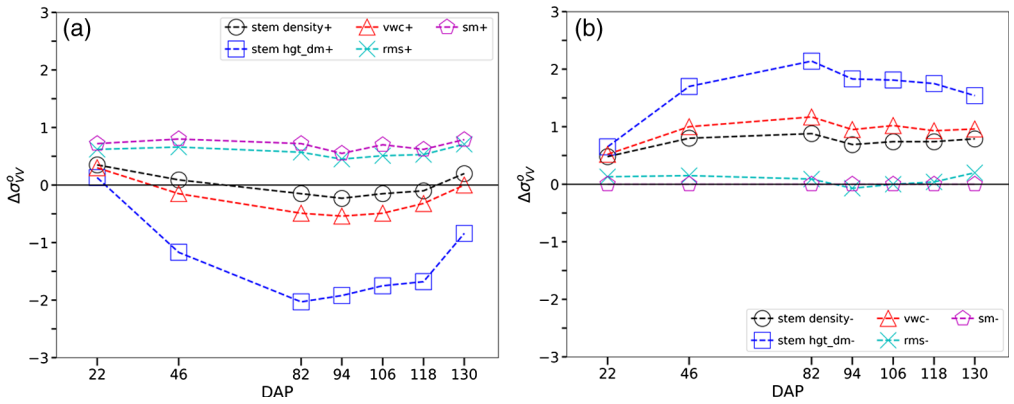

Fig. 10 Backscatter sensitivity response to wheat canopy parameters for (a) +10% varied parameters and (b) −10% varied parameters: stem density (circle-dashed line), stem height, and diameter (stem hgt_dm, square-dashed line), VWC (triangle-dashed line), surface roughness (rms, *x* dashed line), and soil moisture (sm; pentagon-dashed line).

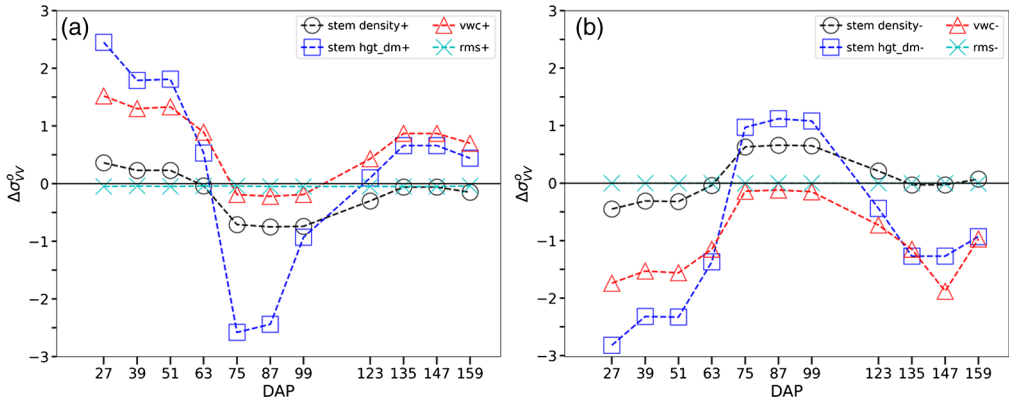

Fig. 11 Backscatter sensitivity response to rice canopy parameters for (a) +10% varied parameters and (b) −10% varied parameters: stem density (circle-dashed line), stem height and diameter (stem hgt_dm, square-dashed line), VWC (triangle-dashed line), and surface roughness (rms, *x* dashed line).

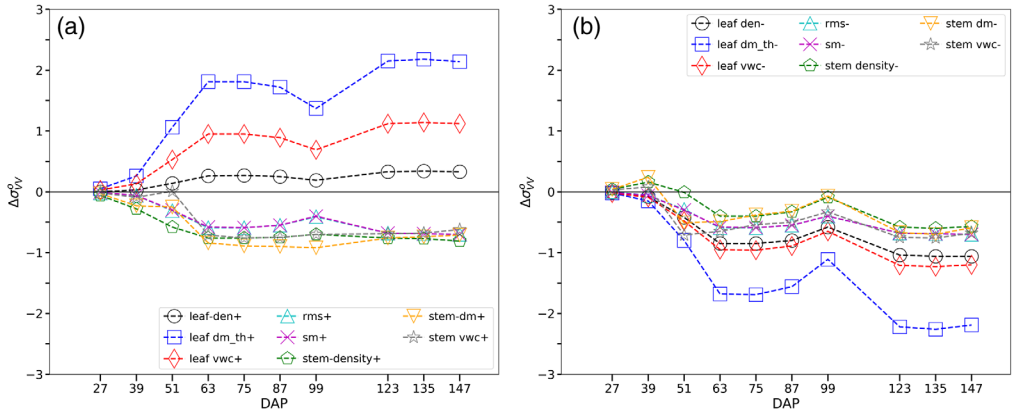

Fig. 12 Backscatter sensitivity response to corn canopy parameters for (a) +10% varied parameters and (b) −10% varied parameters: leaf density (leaf den, circle-dashed line), leaf diameter and thickness (leaf dm_th, square-dashed line), leaf VWC (triangle-dashed line), surface roughness (rms, *x*-dashed line), soil moisture (sm; pentagon-dashed line), stem density (pentagon-dashed line), stem diameter (stem dm, triangle down-dashed line), and stem VWC (star-dashed line).

smaller in magnitude with regard to influence. However, we note that soil moisture values are consistently low throughout the growing season. Additionally, while smaller in magnitude overall, soil moisture may have a larger influence on backscatter depending on the stage of crop development, and hence, the vegetation biomass influences the backscatter sensitivity to soil moisture. For example, in Fig. 10(a) on 22 DAP, when the wheat canopy is not fully developed, a +10% increase in soil moisture produces the largest backscatter response.

Figure 10 shows the backscatter sensitivity response to select wheat vegetation and surface parameters through the growing season. Overall, varying the wheat stem parameters leads to the highest backscatter response (Table 3). An increase (decrease) of the vegetation parameters decreases (increases) radar response. A ±10% parameter change for the stem height, diameter, and both, followed by the VWC produce the largest sensitivity response. Additionally, the −10% stem height and diameter time-series curve is similar to the S1-mean and modeled backscatter curve in Fig. 7. Surface parameters and radar response are directly related to each other with the +10% soil moisture and rms producing a response up to 1 dB. A −10% soil moisture and rms parameters produce a nearly 0 dB sensitivity response. The sensitivity response to increasing soil moisture and rms may explain the S1 σ^0_{VV} spike on 94 DAP. This suggests that some surface feature changed and was observed by Sentinel-1A, but the DSSAT-MIMICS approach is not able to capture that change.

Figure 11 shows the backscatter sensitivity to select rice vegetation and surface parameters. The backscatter response to the rice parameters is not consistent across the growing season. Overall, the varying of the rice stem parameters elicits a greater sensitivity response. Increasing the vegetation parameters leads to a positive sensitivity response before 75 DAP and after 99 DAP. Between DAP 75 and 99, there is an inverse relationship, an increase in the stem parameters leads to a negative sensitivity response. Additionally, the ±10% time-series curve is similar to the stem density curve in Fig. 8. Together, this suggest that (1) stem density dominates the overall magnitude and variation, and (2) the switch to an inverse relationship may be caused by the slightly stronger radar response to the longer and denser rice stems due to the orientation of the stems relative to the VV-polarization, similar to wheat. This suggests σ^0_{VV} is attenuated when the rice canopy is at max height and density, while shorter and thinner rice stems can increase σ^0_{VV} response.

Figure 12 shows the backscatter sensitivity response to select corn vegetation and surface parameters through the growing season. The sensitivity response to leaf parameters is a direct relationship—increasing leaf area leads to a corresponding increase in radar backscatter. The combination of leaf diameter and thickness followed by VWC are the largest influencers for both a ±10% parameter change, up ∼2.5 and 1 dB, respectively. Varying stem and surface parameters have less of an influence and inverse relationship on the backscatter response, the

Table 3 Mean absolute sensitivity response to varied crop parameters for (A) wheat, (B) rice, and (C) corn. Mean absolute sensitivity response expressed as ΔdB.

(A)	Wheat ΔdB
Stem hgt + dm + den	1.87
Stem hgt + dm	1.68
Stem dm	1.38
Stem hgt	1.38
VWC	0.63
Stem density	0.46
SM	0.35
rms	0.34
(B)	**Rice ΔdB**
Stem hgt + dm + den	1.66
Stem hgt + dm	1.52
Stem dm	1.3
Stem hgt	1.19
VWC	0.89
Stem density	0.32
rms	0.02
(C)	**Corn ΔdB**
Leaf hgt + dm + den	1.63
Leaf hgt + dm	1.52
Leaf dm	1.34
Leaf VWC	0.76
Stem dm	0.51
Stem VWC	0.5
Stem density	0.47
rms	0.46
SM	0.46
Leaf den	0.44
Leaf th	0.44
Stem hgt + dm	0.32
Stem hgt + dm + den	0.3
Stem hgt	0.27

increasing of these parameters leads to decreasing radar backscatter. Overall, the slight varying of corn leaf parameters leads to a greater sensitivity response compared to the other corn parameters.

6 SAR Crop Growth Index

The DSSAT-MIMICS modeling approach generates modeled backscatter signatures that represent a particular set of wheat, rice, and corn parameters. Additionally, the modeled backscatter supports interpretation of Sentinel-1A backscatter, identifies the scattering mechanisms contributing to total backscatter, and accounts for differences in backscatter associated with crop and surface parameters. This supports the comparison of S1 backscatter from the wheat, rice, and corn fields to modeled backscatter signatures, or reference backscatter, to understand field variability. Measured backscatter variation from a baseline modeled reference backscatter can be mainly attributed to crop vegetation parameters influencing backscatter, specifically the structures, based on the sensitivity analysis. Using this information, we calculate the difference between the ensemble mean Sentinel-1A σ^0_{VV} and DSSAT-MIMICS modeled σ^0_{VV}, the reference backscatter, for the SAR CGI, expressed as in Eq. 4. We apply the SAR CGI to map wheat, rice, and corn within-field variability (Fig. 13). For each crop, different DAPs were selected for application.

Wheat mean SAR CGI is 0.33 dB with 55% of the field areas having high growth conditions relative to the reference backscatter (>0 dB) on 82 DAP [Fig. 13(a)]. Backscatter from 21% of the field areas was 2 dB above the DSSAT-MIMICS reference backscatter, suggesting higher growth conditions. About 37% of the wheat field areas were within 1 dB of the reference backscatter. In relation to the sensitivity response, a variation of 1 dB suggests a $\pm 10\%$ growth variation from wheat parameters modeled. Corn field areas on 75 DAP mean SAR CGI is -0.72 dB with 40% of the areas within 1 dB of the reference backscatter, suggesting a $\pm 10\%$ growth variation from corn parameters modeled [Fig. 13(c)]. A fair amount of the fields had low growth conditions, where 65% of the field areas were below the DSSAT-MIMICS reference backscatter. This suggests corn growth lagged in certain areas. Rice fields on 63 DAP mean CGI is -0.28 dB, with 30% of the areas within 1 dB of the reference backscatter and 45% were above the reference (>0 dB), suggesting higher rice growth in some of the field areas [Fig. 13(e)].

Wheat mean SAR CGI is 0.56 dB and 68% of the field areas had high growth conditions relative to the DSSAT-MIMICS reference backscatter on 130 DAP [Fig. 13(b)]. About 40% of the wheat fields are within 1 dB of the reference backscatter, suggesting a $\pm 10\%$ growth variation from wheat parameters modeled. Only 29% of the corn field areas are within 1 dB of the DSSAT-MIMICS reference backscatter on 135 DAP [Fig. 13(d)]. A fair amount of the corn field areas displayed low growth conditions. The rice fields on 135 DAP mean SAR CGI is -0.33 dB, with 41% of the field areas within 1 dB of the reference backscatter and 43% are above 0 dB, suggesting higher growth conditions relative to the DSSAT-MIMICS reference backscatter.

The negative SAR CGIs on different DAPs show that measured backscatter from these areas lagged behind what was expected based on DSSAT-MIMICS simulations, suggesting suboptimal crop growth in these areas. This could be a result of the actual planting dates differing from the DSSAT planting dates, or plant stresses occurring in the field (e.g., nutrient, water, and pest) but not captured by DSSAT. Positive SAR CGIs indicate crop growth that was ahead than what was expected based on DSSAT-MIMICS reference backscatter. This could indicate slightly earlier planting dates or ideal conditions that created higher wheat, rice, and corn growth. In this study, we use a single DSSAT-MIMICS simulation as a backscatter reference for multiple fields observed by Sentinel-1A. Future assessments with SAR CGI could run DSSAT-MIMICS for each field.

7 Discussion

S1 mean backscatter for the wheat and rice fields displayed similarity within each other in Figs. 7 and 8. This suggests wheat and rice fields were developing at similar rates, but the amount of vegetation varied based on the differing S1 backscatter values. S1 mean backscatter for the corn

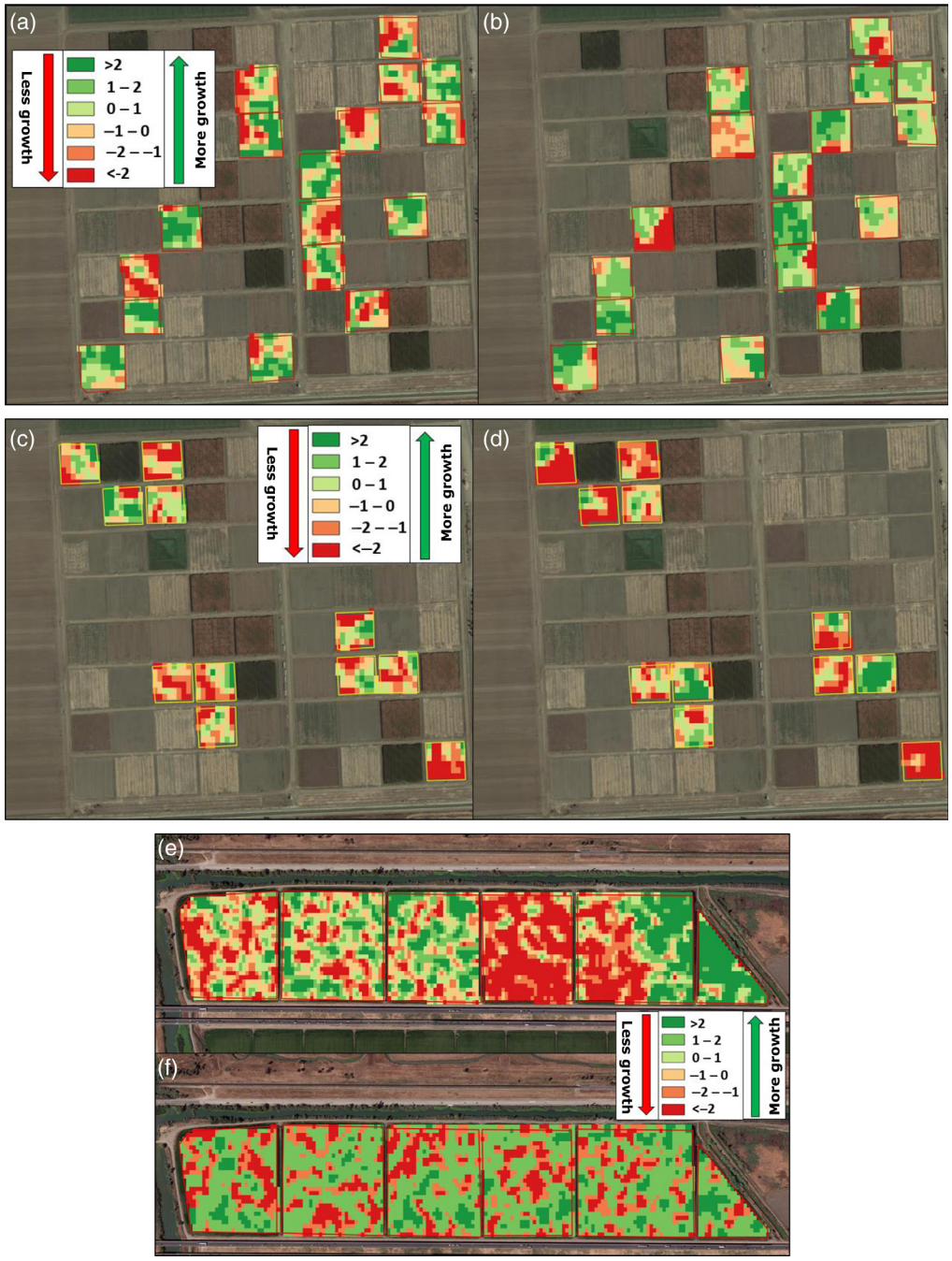

Fig. 13 SAR CGI maps for wheat, rice, and corn field area variability on specific DAPs (with S1 observation date). (a) Wheat fields at Russell Ranch on 82 DAP (S1 date February 5, 2015). (b) Wheat fields at Russell Ranch on 130 DAP (S1 date March 25, 2015). (c) Corn fields at Russell Ranch on 75 DAP (S1 date June 29, 2015). (d) Corn fields at Russell Ranch on 75 DAP (S1 date August 25, 2015). (e) Rice fields in eastern Yolo County on 63 DAP (S1 date June 17, 2015). (f) Rice fields in eastern Yolo County on 135 DAP (S1 date August 28, 2015). SAR CGI legend provided in each image.

fields had a higher degree of variation relative to other crops, suggesting the amount of vegetation varied through the growing season. By combining S1 backscatter, the mean ensemble backscatter represents the average conditions for each crop. This was used to identify VWCs that, with wheat, rice, and corn parameters inputs for MIMICS, represented a certain modeled backscatter signature.

The wheat field analysis (Fig. 7), DSSAT-MIMICS modeled σ^0_{VV} was strongly correlated with ensemble mean S1 σ^0_{VV} with an RMSE dB and Esys <2 dB. This evaluation is consistent with previously published work.[9,25] The time-series and sensitivity analyses highlighted the attenuation effects the wheat canopy can have on radar response (Figs. 7 and 10; Table 3). Similar attenuating effects were reported.[9,18–20] MIMICS identified direct ground scattering as the main contributor to total backscatter, similar to previously published work that modeled a wheat canopy to interpret the scattering physics.[9,25] However, the retrieved wheat stem VWCs did not produce the dynamic VWC range seen in a developing wheat field.[25] This may be due to the direct ground contribution dominating the total backscatter in addition to backscatter sensitivity to stem geometry, making the determination of stem VWCs difficult during the wheat growing season.

In the rice analysis, DSSAT-MIMICS modeled σ^0_{VV} is strongly correlated with the ensemble mean S1 σ^0_{VV} and produced an RMSE <2 dB and an Esys close to 0 dB (Fig. 8). MIMICS modeled σ^0_{VH} was not statistically correlated to S1 σ^0_{VH} and produced higher RMSE and *E*sys compared to σ^0_{VV}, which is difficult to address because of the lack of Sentinel-1A σ^0_{VH} observations. DSSAT-MIMICS σ^0_{VV} and σ^0_{VH} backscatter was dominated by the ground-canopy (ground-canopy or water-stem) scattering contribution, similar to Ref. 23. The sensitivity analysis reveals radar response varied as the rice canopy develops. When the rice canopy is developing or thinning, the sensitivity response varied directly with any change in rice parameters (Fig. 11). This differs when the rice canopy reached a certain density and stem height, leading to an attenuation effect. In Ref. 23, a sensitivity response was performed for the entire rice growing season and found an inverse relation between rice stem parameters and backscatter response. Similar attenuation effects on radar as the rice canopy matured was reported in Ref. 22. This suggests the attenuation effect may occur when the rice canopy reaches a certain density and height. Finally, DSSAT-MIMICS was able to estimate rice stem VWCs that produced a range of values in developing rice fields.[65,66]

For the corn analysis (Fig. 9), DSSAT-MIMICS modeled σ^0_{VV} was correlated to the ensemble mean S1 σ^0_{VV} and produced an RMSE close to 1 dB and Esys close to 0 dB. DSSAT-MIMICS modeled σ^0_{VH} was not statistically significant to S1 σ^0_{VH} and produced slightly higher RMSE dB and Esys. The RMSEs are similar to those found by Ref. 9. The modeled backscatter for both polarizations identified the ground as the main contributor to total backscatter during early corn growth and the canopy as the main contributor as the corn canopy matured [LAI surpasses 3; Fig. 9(c)]. The sensitivity analysis performed reveals radar response is sensitive to changing corn leaf parameters (Fig. 12; Table 3). The retrieved corn stem and leaf VWCs fall within previously reported corn moisture measurements and display similar variations previously reported (Fig. 6[64,67]).

Using the information from the analyses, the SAR CGI identified field areas of high and low growth relative to the DSSAT-MIMICS reference backscatter values (Fig. 13). The wheat fields generally displayed high growth conditions relative to the reference backscatter value, suggesting field areas more developed relative to the wheat growth simulated in the DSSAT-MIMICS approach. For rice, during the early growth stage, the field areas displayed a high amount of heterogeneity that reduced in the later growth stage. The corn fields had areas that experienced negative index values, indicating certain areas were underdeveloped relative to the corn growth simulated in DSSAT-MIMICS approach.

8 Conclusion

This study developed and evaluated a combined DSSAT-MIMICS modeling approach to assess wheat, rice, and corn field growth variability observed by Sentinel-1A for water year 2015 in Yolo County, California. We applied this methodology to inform on crop growth and development by relating Sentinel-1A backscatter to the DSSAT-MIMICS modeled backscatter signature that simulated specific wheat, rice, and corn parameters and growth. Our findings support five main conclusions.

1. DSSAT-MIMICS was able to simulate Sentinel-1A σ^0_{VV} for wheat, rice, and corn and both are strongly correlated. For σ^0_{VH}, the seasonal change between modeled and

S1 backscatter was similar but limited because of the lack of cross-polarization acquisitions during water year 2015.
2. Wheat VWC estimates were realistic on average, consistent with results from prior studies, but do not reflect the expected seasonal variability in vegetation moisture. Rice VWC estimates generally captured the moisture changes found in previous studies. Corn VWCs have reasonable variations but have lower VWCs during early corn growth and slightly higher VWCs for late corn growth relative to prior results.
3. Radiometric modeling using MIMICS identified major contributors to total backscatter for each polarization by crop type, consistent with previous studies. Direct ground scattering dominated total backscatter for wheat. Canopy-ground scattering was the dominant contributor to total backscatter for rice. For corn, the direct ground scattering contribution diminished while direct canopy scattering contribution increased as the canopy developed.
4. Modeled C-band backscatter was sensitive to wheat stem parameters and decreased with crop development. Modeled C-band backscatter for rice was most sensitive to the rice stem parameters. Modeled C-band backscatter for mature corn was most sensitive to the leaf parameters.
5. SAR CGI demonstrated potential to assess crop development by identifying areas that exhibited high or low growth relative to a consistently modeled reference backscatter.

Our approach would benefit from more time-series Sentinel-1A cross-polarization observations, which could help constrain and adjust the unexpected VWCs. A more consistent cross-polarized backscatter time-series would also support interpretation of radar response to the vegetation volume. A dual-frequency approach wherein C-band SAR would be combined with L-band SAR, would also enhance characterization of canopy conditions.

DSSAT-MIMICS and SAR CGI show potential for providing information on growth status and within- and between-field variability. A low or very low growth index could be an indicator of vegetation stress or delayed growth because of later planting dates. A better understanding of how to differentiate stress and growth as measured by SAR is needed to refine this index and verify the ability of DSSAT-MIMICS to assess canopy conditions.

While we present a proof of concept in this paper, extending the DSSAT-MIMICS analysis to multiple years and over multiple regions would advance the usability and potential of this approach. An analysis of this approach should be applied to different SAR platforms to understand the utility of monitoring crops using the DSSAT-MIMICS approach. As a next step, DSSAT could simulate different crop conditions to generate the resultant parameters that represent healthy and stressed crop conditions by varietal. The resultant parameters can be used in MIMICS to model healthy and stressed crop backscatter signatures and can be compared to different SAR measurements to understand how the SAR response differs from DSSAT-MIMICS modeled responses. Since DSSAT, MIMICS, and SAR CGI are flexible and adaptable, this provides the opportunity to monitor crops at large-scale without the need to be in those fields. The only information needed is meteorological data, crop location and type, and a general growth window. This creates the opportunity to expand our crop monitoring efforts for improved monitoring, forecasting, and possibly yield estimates in different agricultural regions.

Acknowledgments

This work was supported by the NASA Applied Sciences Program (Grant No. NNH11ZDA001N-WATER) and National Science Foundation (Grant No. BCS 184018).

References

1. Y. Inoue and E. Sakaiya, "Relationship between X-band backscattering coefficients from high-resolution satellite SAR and biophysical variables in paddy rice," *Remote Sens. Lett.* **4**(3), 288–295 (2013).

2. C. Hütt and G. Waldhoff, "Multi-data approach for crop classification using multitemporal, dual-polarimetric TerraSAR-X data, and official geodata," *Eur. J. Remote Sens.* **51**(1), 62–74 (2018).
3. H. McNairn and J. Shang, "A review of multitemporal synthetic aperture radar (SAR) for crop monitoring," in *Multitemporal Remote Sensing*, Y. Ban, Ed., Springer, Cham, pp. 317–340 (2016).
4. S. Frolking et al., "Evaluation of the SeaWinds scatterometer for regional monitoring of vegetation phenology," *J. Geophys. Res.: Atmos.* **111**(D17), D17302 (2006).
5. A. Navarro et al., "Crop monitoring based on SPOT-5 Take-5 and sentinel-1A data for the estimation of crop water requirements," *Remote Sens.* **8**(6), 525 (2016).
6. G. Wiseman et al., "RADARSAT-2 polarimetric SAR response to crop biomass for agricultural production monitoring," *IEEE J. Sel. Top. Appl. Earth Obs. Remote Sens.* **7**(11), 4461–4471 (2014).
7. Y. Shao et al., "Rice monitoring and production estimation using multitemporal RADARSAT," *Remote Sens. Environ.* **76**(3), 310–325 (2001).
8. H. S. Srivastava et al., "Potential applications of multi-parameteric synthetic aperture radar (SAR) data in wetland inventory: a case study of Keoladeo National Park (A World Heritage and Ramsar site), Bharatpur, India," in *2007, Proc. 12th World Lake Conf., TAAL*, Jaipur, India (2008).
9. A. Della Vecchia et al., "Influence of geometrical factors on crop backscattering at C-band," *IEEE Trans. Geosci. Remote Sens.* **44**(4), 778–790 (2006).
10. S. C. Steele-Dunne et al., "Radar remote sensing of agricultural canopies: a review," *IEEE J. Sel. Top. Appl. Earth Obs. Remote Sens.* **10**(5), 2249–2273 (2017).
11. N. Baghdadi et al., "Multitemporal observations of sugarcane by TerraSAR-X images," *Sensors* **10**(10), 8899–8919 (2010).
12. M. W. Whitt and F. T. Ulaby. "Radar response of periodic vegetation canopies," *Int. J. Remote Sens.* **15**(9), 1813–1848 (1994).
13. P. Patel, H. S. Srivastava, and R. R. Navalgund. "Estimating wheat yield: an approach for estimating number of grains using cross-polarised ENVISAT-1 ASAR data," *Proc. SPIE* **6410**, 641009 (2006).
14. F. T. Ulaby and T. Bush, "Corn growth as monitored by radar," *IEEE Trans. Antennas Propag.* **24**(6), 819–828 (1976).
15. F. T. Ulaby et al., "Relating the microwave backscattering coefficient to leaf area index," *Remote Sens. Environ.***14**(1–3), 113–133 (1984).
16. X. Jiao et al., "The sensitivity of RADARSAT-2 polarimetric SAR data to corn and soybean leaf area index," *Can. J. Remote Sens.* **37**(1), 69–81 (2011).
17. F. T. Ulaby and D. Long, *Microwave Radar and Radiometric Remote Sensing*, Artech House (2015).
18. S. Paloscia et al., "The potential of C-and L-band SAR in estimating vegetation biomass: the ERS-1 and JERS-1 experiments," *IEEE Trans. Geosci. Remote Sens.* **37**(4), 2107–2110 (1999).
19. F. Mattia et al., "Multitemporal C-band radar measurements on wheat fields," *IEEE Trans. Geosci. Remote Sens.* **41**(7), 1551–1560 (2003).
20. A. Balenzano et al., "Dense temporal series of C-and L-band SAR data for soil moisture retrieval over agricultural crops," *IEEE J. Sel. Top. Appl. Earth Obs. Remote Sens.* **4**(2), 439–450 (2011).
21. T. Le Toan et al., "Rice crop mapping and monitoring using ERS-1 data based on experiment and modeling results," *IEEE Trans. Geosci. Remote Sens.* **35**(1), 41–56 (1997).
22. Y. Oh et al., "Polarimetric backscattering coefficients of flooded rice fields at L- and C-bands: measurements, modeling, and data analysis," *IEEE Trans. Geosci. Remote Sens.* **47**(8), 2714–2721 (2009).
23. Y. Liu et al., "Modeling and characteristics of microwave backscattering from rice canopy over growth stages," *IEEE Trans. Geosci. Remote Sens.* **54**(11), 6757–6770 (2009).
24. K. C. McDonald, M. C. Dobson, and F. T. Ulaby, "Using MIMICS to model L-band multiangle and multitemporal backscatter from a walnut orchard," *IEEE Trans. Geosci. Remote Sens.* **28**(4), 477–491 (1990).

25. A. Toure et al., "Adaptation of the MIMICS backscattering model to the agricultural context-wheat and canola at L and C bands," *IEEE Trans. Geosci. Remote Sens.* **32**(1), 47–61 (1994).
26. A. Monsivais-Huertero and J. Judge, "Comparison of backscattering models at L-band for growing corn," *IEEE Geosci. Remote Sens. Lett.* **8**(1), 24–28 (2010).
27. K. C. McDonald, *Modeling Microwave Backscatter from Tree Canopies,* University of Michigan (1991).
28. J. Y. Koay et al., "Paddy fields as electrically dense media: Theoretical modeling and measurement comparisons," *IEEE Trans. Geosci. Remote Sens.* **45**(9), 2837–2849 (2007).
29. M. Hosseini et al., "Estimation of Leaf Area Index (LAI) in corn and soybeans using multipolarization C-and L-band radar data," *Remote Sens. Environ.* **170**, 77–89 (2015).
30. D. Han et al., "Crop water content of winter wheat revealed with Sentinel-1 and Sentinel-2 imagery," *Sensors* **19**(18), 4013 (2019).
31. J. M. Winter et al., "Integrating water supply constraints into irrigated agricultural simulations of California," *Environ. Modell. Software* **96**, 335–346 (2017).
32. V. K. Mehta et al., "Irrigation demand and supply, given projections of climate and land-use change, in Yolo County, California," *Agric. Water Manage.* **117**, 70–82 (2013).
33. K. M. Wolf et al., "The century experiment: the first twenty years of UC Davis' Mediterranean agroecological experiment," 2018, http://asi.ucdavis.edu/programs/rr.
34. USDA-NASS, USDA National Agricultural Statistics Service Cropland Data Layer. 2020, https://nassgeodata.gmu.edu/CropScape/ (2018).
35. ESA 2018, "Sentinel-1 SAR User Guide Introduction [http://www.esa.int/]," 2017 https://sentinel.esa.int/web/sentinel/user-guides/sentinel-1-sar/applications.
36. Copernicus Sentinel Data 2015, Retrieved from ASF DAAC (15 November 2018), processed by ESA https://www.asf.alaska.edu/.
37. J. M. Peña-Barragán et al., "Object-based crop identification using multiple vegetation indices, textural features and crop phenology," *Remote Sens. Environ.* **115**(6), 1301–1316 (2011).
38. USDA NASS, "Field crops: usual planting and harvesting dates," in *USDA National Agricultural Statistics Service, Agricultural Handbook*, Vol. **628**, U.S. Department of Agriculture (USDA) (2010).
39. SNAP–ESA Sentinel Application Platform, http://step.esa.int.
40. G. Hoogenboom et al., *Decision Support System for Agrotechnology Transfer (DSSAT) Version 4.5 [CD-ROM]*, University of Hawaii, Honolulu, Hawaii (2012).
41. J. W. Jones et al., "The DSSAT cropping system model," *Eur. J. Agron.* **18**(3–4), 235–265 (2003).
42. L. O. Mearns, C. Rosenzweig, and R. Goldberg, "The effect of changes in daily and interannual climatic variability on CERES-Wheat: a sensitivity study," *Clim. Change* **32**(3), 257–292 (1996).
43. M. Parry, C. Rosenzweig, and M. Livermore, "Climate change, global food supply and risk of hunger," *Philos. Trans. R. Soc. Lond. Ser. B, Biol. Sci.* **360**(1463), 2125–2138 (2005).
44. C. Rosenzweig et al., "Assessing agricultural risks of climate change in the 21st century in a global gridded crop model intercomparison," *Proc. Natl. Acad. Sci. U. S. A.* **111**(9), 3268–3273 (2014).
45. S. Asseng et al., "Uncertainty in simulating wheat yields under climate change," *Nat. Clim. Change* **3**(9), 827 (2013).
46. J. R. Lopez et al., "Integrating growth stage deficit irrigation into a process based crop model," *Agric. For. Meteorol.* **243**, 84–92 (2017).
47. K. Brumbelow and A. Georgakakos, "An assessment of irrigation needs and crop yield for the United States under potential climate changes," *J. Geophys. Res.: Atmos.* **106**(D21), 27383–27405 (2001).
48. R. Greenwald et al., "The influence of aerosols on crop production: a study using the CERES crop model," *Agric. Syst.* **89**(2–3), 390–413 (2006).
49. D. B. Lobell and J. I. Ortiz-Monasterio, "Impacts of day versus night temperatures on spring wheat yields," *Agron. J.* **99**(2), 469–477 (2007).
50. California Irrigation Management Information System (CIMIS), https://cimis.water.ca.gov.

51. C. D. Keeling et al., "Exchanges of atmospheric CO_2 and $13CO_2$ with the terrestrial biosphere and oceans from 1978 to 2000. I. Global aspects," (2001).
52. C. Frate and L. Schwanki, "Crop irrigation strategies: corn [Homepage of University of California]," 2018, http://ucmanagedrought.ucdavis.edu/Agriculture/Crop_Irrigation_Strategies/Corn/ (accessed 24 November 2014).
53. L. Jackson et al., "Small grain production manual (complete)," https://ucanr.edu (2006).
54. D. Geisseler and W. R. Horwath, "Rice production in California," in *Fertilizer Research and Education Program*, pp. 1–3, Department of Land, Air and Water Resources at the University of California, Davis (2013).
55. L. Espino, M. Leinfedler-Miles, and C. Mutters, *Rice Production Manual*, 15th edn., University of California, Division of Agriculture and Natural Resources (2015).
56. P. Steduto et al., "FAO Irrigation and drainage paper 66," in *Crop Yield Response to Water*, Food and Agriculture Organization of the United Nations (2012).
57. J. M. Lopez-Sanchez, J. D. Ballester-Berman, and I. Hajnsek, "Rice monitoring in Spain by means of time-series of TerraSAR-X dual-pol images," in *Proc. Int. Workshop. Appl. Polarimetry Polarimetric Interferometry (Pol-InSAR)*, Frascati, p. 26 (2009).
58. R. Klein, "How winter Wheat seeding date can have a major effect on yields, [Homepage of University of Nebraska-Lincoln, Institute of Agriculture and Natural Resources]," 2017, https://cropwatch.unl.edu/2017/how-winter-wheat-seeding-date-can-have-major-effect-yields.
59. Y. Oh, K. Sarabandi, and F.T. Ulaby, "An empirical model and an inversion technique for radar scattering from bare soil surfaces," *IEEE Trans. Geosci. Remote Sens.* **30**(2), 370–381 (1992).
60. R. Panciera et al., "Evaluation of IEM, Dubois, and Oh radar backscatter models using airborne L-band SAR," *IEEE Trans. Geosci. Remote Sens.* **52**(8), 4966–4979 (2013).
61. M. Choker et al., "Evaluation of the Oh, Dubois and IEM backscatter models using a large dataset of SAR data and experimental soil measurements," *Water* **9**(1), 38 (2017).
62. F. T. Ulaby and M. A. El-Rayes, "Microwave dielectric spectrum of vegetation—Part II: dual-dispersion model," *IEEE Trans. Geosci. Remote Sens.* **GE-25**, 550–557 (1987).
63. M. T. Hallikainen et al., "Microwave dielectric behavior of wet soil—part 1: Empirical models and experimental observations," *IEEE Trans. Geosci. Remote Sens.* **GE-23**, 25–34 (1985).
64. C. Igathinathane et al., "Mass and moisture distribution in aboveground components of standing corn plants," *Trans. ASABE* **49**(1), 97–106 (2006).
65. M. Jia et al., "Rice biomass estimation using radar backscattering data at S-band," *IEEE J. Sel. Top. Appl. Earth Obs. Remote Sens.* **7**(2), 469–479 (2014).
66. L. Tan et al., "Rice biomass retrieval from advanced synthetic aperture radar image based on radar backscattering measurement," *J. Appl. Remote Sens.* **9**(1), 097091 (2015).
67. A. Monsivais-Huertero, P.-W. Liu, and J. Judge, "Phenology-based backscattering model for corn at L-band," *IEEE Trans. Geosci. Remote Sens.* **56**(9), 4989–5005 (2018).

Aaron Davitt received his BA degree in ecology from the University of Denver in 2006 and an MA degree in geology from City College of New York in 2011, followed by his PhD from the Graduate Center, City University of New York in 2020. His research specialization includes combining optical-IR, thermal IR, and active and passive microwave remote sensing data to inform on crop stress and growth, and radiometric modeling of crop canopies.

Jonathan M. Winter is an assistant professor at the Department of Geography at Dartmouth College, Hanover, New Hampshire. His research interests include climate prediction, agricultural modeling, and climate impacts on water resources and food security.

Kyle McDonald is Terry Elkes Professor in the Earth and Atmospheric Sciences Department, City College of New York, and part-time faculty in the Carbon Cycle and Ecosystems Group at the Jet Propulsion Laboratory, California Institute of Technology. Prior to joining City College in 2011, he was a principal scientist in JPL's Water and Carbon Cycles Group. He specializes in microwave remote sensing of terrestrial ecosystems and is a member of NASA's NISAR Science Team.